Electronic Research Archive

http://www.aimspress.com/journal/era

ERA, 33(8): 4693–4722.
DOI: 10.3934/era.2025211
Received: 13 June 2025
Revised: 20 July 2025
Accepted: 25 July 2025
Published: 14 August 2025

Research article

Active vibration control for fractional order systems based on multiple region eigenvalue assignment

Binxin He[1] **and Hao Liu**[1,2,*]

[1] School of Mathematics, Nanjing University of Aeronautics and Astronautics, Nanjing 211106, China

[2] Shenzhen Research Institute, Nanjing University of Aeronautics and Astronautics, Shenzhen 518110, China

* **Correspondence:** Email: hliu@nuaa.edu.cn.

Abstract: This work addresses active vibration control for fractional-order systems based on a multiple region eigenvalue assignment. First, we propose the selection criteria of fractional-order multiple stability regions and define multiple stability regions by generalized linear matrix inequality. Based on the inverse eigenvalue problem theory, we give the sufficient condition for solving the feedback control matrix under multiple region eigenvalue assignment and present the expression of the feedback control matrix. Then, we propose a numerical algorithm for solving this problem, which improves the control performance. Finally, we verify the feasibility and effectiveness of the proposed method through numerical examples of fractional-order simulation and actual physical systems.

Keywords: fractional derivative model; active vibration control; region eigenvalue assignment; linear matrix inequality; inverse eigenvalue problem

1. Introduction

We consider the following fractional-order linear system in the state-space form:

$$D^{\alpha}x(t) = Ax(t) + Bu(t), \tag{1.1}$$

where $A \in \mathbb{R}^{n\times n}$ is the system matrix, $x(t) \in \mathbb{R}^n$ is the state variable, $B \in \mathbb{R}^{n\times l}$ is the control matrix, $u(t) \in \mathbb{R}^l$ is the control input vector, and D^{α} $(0 < \alpha < 2)$ is the fractional-order derivative. Since fractional derivatives can be used to describe hereditary properties and long memory transients of the behavior of various natural phenomena, several control systems in the real world can be described by fractional-order models, such as viscoelastic systems [1], neuronal systems [2], supercapacitors or

hybrid systems [3], and unmanned aircraft systems [4]. Additionally, many fractional-order derivatives have been combined with nonlinear partial differential equations to form fractional-order partial differential models, which are important research objects in the field of nonlinear optics and applied science [5]. The dynamic property of these fractional-order partial differential models has been investigated in [6, 7]. In recent research, the impacts of fractional-order systems have expanded across various domains, including flight control theory [8], bioengineering [9], and electronic circuits [10].

Vibrations are inevitably generated due to rotation and working of components during the operation of fractional-order systems, which affect the stability of the system. Passive and active vibration control are the primary methods for reducing vibrations. Passive vibration control reduces vibration by placing devices in the structures [11, 12]. However, it cannot be adjusted with the system state, resulting in limited flexibility and inconspicuous control effect. Active vibration control [13], in contrast to passive methods, depends on feedback control through actuating sensors to reduce vibration. It can offer greater flexibility and adaptability to varying external conditions. In [14], a diffusion collaboration-based distributed Filtered-x Least Mean Square algorithm was applied to active vibration control to address the issue of increased control scale. In [15], Zhang et al. investigated active vibration control of aircraft wings under dynamic loading by using a constant-gain negative velocity feedback control technique, which enhanced prediction accuracy and control efficiency. In [16], an active vibration control method based on proportional integral-linear quadratic regulator state feedback was studied to suppress the vibration of ship pipeline systems. In [17], the classical proportional integral derivative program was employed to scrutinize the efficacy of closed-loop active vibration control. In [18], Tian et al. researched the active control of the shaft-shell system of an underwater vehicle. Additionally, the active vibration control method was also applied to a novel fractional-order chaotic jerk system [19]. Therefore, active vibration control for fractional-order systems requires designing a controller $u(t)$ to reduce vibration and preserve the stable system performance. The common state feedback control is expressed by

$$u(t) = Fx(t), \tag{1.2}$$

where $F \in \mathbb{R}^{l\times n}$ is the feedback control matrix. Then, the closed-loop system can be expressed as

$$D^{\alpha}x(t) = (A + BF)x(t). \tag{1.3}$$

We aim to find the feedback control matrix such that the system (1.3) maintains stability performance. The process of active vibration control for fractional-order systems is demonstrated in Figure 1.

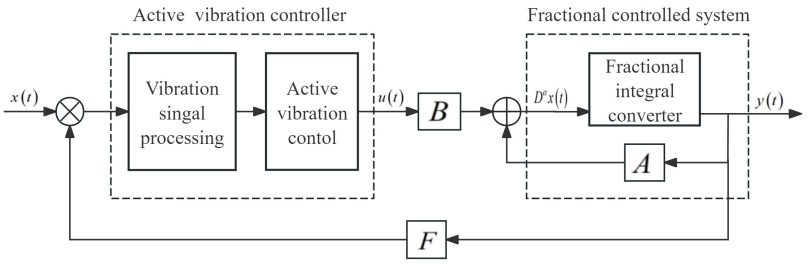

Figure 1. The process diagram of active vibration control.

The closed-loop system performance is determined by closed-loop eigenvalues [20], and region eigenvalue assignment is a widely used controller design method to improve control system performance [21]. In [22], Zhang et al. evaluated the design of the fault detection filter using regional pole assignment in an uncertain linear discrete-time system. In [23], Richiedei and Tamellin proposed a novel approach for solving regional pole placement for linear systems by state feedback control. In [24], Schaub et al. developed the method for designing robust controllers based on a region eigenvalue assignment. In [25], Arıcan et al. introduced a new state-dependent regional pole assignment method for nonlinear systems, which produced a state-dependent feedback control law enabling the eigenvalues of the closed-loop matrix to be placed in a specified disk. Furthermore, they proposed two algorithms to update the disc parameters for improving stability in [26]. In [27], region stability and H_∞ optimization control for discrete-time impulsive Takagi–Sugeno fuzzy systems were studied, where the proposed method maintained the stability of the system while simultaneously addressing constraints on convergence speed and damping response. More related references can be seen in [28, 29].

Most of above research focus on a single region to assign all the eigenvalues, which cannot adjust system performance flexibly. In [30], a method for designing an optimal tracking control scheme through multiple-region pole assignment was presented, which motivated our work. With the aim assign closed-loop eigenvalues of fractional-order system (1.1) from a single region to multiple regions, each eigenvalue is assigned to a specified region. Hence, active vibration control for fractional-order systems based on multiple region eigenvalue assignment can be mathematically described as:

Problem MREAP: For a given fractional-order system (1.1) and multiple specified regions, find the feedback control matrix F such that all the eigenvalues of the closed-loop system matrix $A + BF$ are in specified multiple regions.

Based on the multiple region eigenvalue assignment method, a feedback control matrix is designed in our study for active vibration control of fractional-order systems. The main contributions of this paper are as follows:

- Compared with single-region eigenvalue assignment, we present the selection criteria of fractional-order multiple stability regions based on linear matrix inequality theory.
- Based on the inverse eigenvalue problem theory, we give the sufficient conditions for solving the feedback control matrix under multiple-region eigenvalue assignment and present the expression of the feedback control matrix.
- We propose a numerical algorithm for solving the active vibration control problem of fractional-order systems, which improves control performance.

The following sections of this work are organized as follows. In Section 2, the selection criteria of fractional-order multiple stability regions and the definition of multiple stability regions by generalized linear matrix inequality are proposed. Subsequently, we present the sufficient conditions for solving the feedback control matrix under the multiple-region eigenvalue assignment and propose a numerical algorithm for solving this problem in Section 3. Finally, fractional-order simulation and actual physical experimental results are given to illustrate the effectiveness of our approach in Section 4.

Notations: A^T, $\bar{A}$, and A^H denote the transpose, conjugate, and conjugate transpose of matrix A, respectively. "> 0" represents positive definite and "< 0" represents negative definite. $\otimes$ denotes the Kronecker product. I represents the identity matrix with appropriate dimensions.

2. Selection criteria for fractional-order multiple stability regions

The traditional methods describes the stability region in the form of linear matrix inequality (LMI), which is limited to describing a convex subregion. Next, we will introduce the definition of the generalized linear matrix inequality (GLMI) region, which generalizes the traditional description to a region including, but not limited to, convexity.

Definition 2.1. [31] *A GLMI region $\mathscr{D}_R$ is a subset in the complex plane defined as*

$$\mathscr{D}_R = \left\{ s \in \mathbb{C} : f_{\mathscr{D}_R}(s) = H_{11} + sH_{12} + \bar{s}H_{12}^H + s\bar{s}H_{13} < 0 \right\}, \tag{2.1}$$

where $H_{11} = H_{11}^H \in \mathbb{C}^{d\times d}$, $H_{12} \in \mathbb{C}^{d\times d}$, $H_{13} = H_{13}^H \in \mathbb{C}^{d\times d}$. The function

$$f_{\mathscr{D}_R}(s) = H_{11} + sH_{12} + \bar{s}H_{12}^H + s\bar{s}H_{13} \tag{2.2}$$

is the characteristic function of the GLMI region $\mathscr{D}_R$.

From Definition 2.1, it is clear that $\mathscr{D}_R$ takes LMI form when $H_{13} = 0$, meaning that the LMI region can be regarded as a special case of the GLMI region.

For fractional-order system (1.1), the stability region is shown in Figure 2. We can observe that the stability region is $\mathscr{D}_s = \mathscr{D}_{R_1} \cup \mathscr{D}_{R_2}(\delta_1 = \delta_2 = (1-\alpha)\pi/2)$ when $0 < \alpha < 1$, which includes a part of the right half complex plane and is nonconvex. When $1 \le \alpha < 2$, the stability region is $\mathscr{D}_s = \mathscr{D}_{R_1} \cap \mathscr{D}_{R_2}(\delta_1 = \delta_2 = (\alpha-1)\pi/2)$ [32].

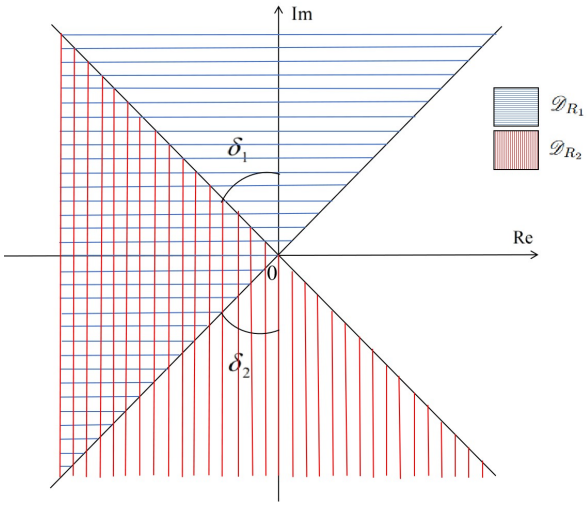

Figure 2. The stability region of the fractional-order system.

According to Definition 2.1, $\mathscr{D}_{R_1}$ and $\mathscr{D}_{R_2}$ can be described as [32]

$$\mathscr{D}_{R_1} = \left\{ s \in \mathbb{C} : f_{\mathscr{D}_{R_1}}(s) = s(\sin(\alpha\pi/2) + i\cos(\alpha\pi/2)) + \bar{s}(\sin(\alpha\pi/2) - i\cos(\alpha\pi/2)) < 0 \right\}, \tag{2.3}$$

$$\mathscr{D}_{R_2} = \left\{ s \in \mathbb{C} : f_{\mathscr{D}_{R_2}}(s) = s(\sin(\alpha\pi/2) - i\cos(\alpha\pi/2)) + \bar{s}(\sin(\alpha\pi/2) + i\cos(\alpha\pi/2)) < 0 \right\}. \tag{2.4}$$

Under the premise of the stability region description of fractional-order systems, we will introduce the selection criteria for fractional-order multiple stability regions to assign closed-loop eigenvalues.

Without loss of generality, we take the case $0 < \alpha < 1$ as an example. In practical applications, one of the most important considerations in the selection criteria of multiple regions is the selection of the region shape and location, as they have a great effect on the system response and control effort [26]. Hence, taking into account the demand of simplicity in the description, we take circle regions to assign closed-loop eigenvalues, which is one of the most used bounded regions.

For the fractional-order system with the eigenvalue $\lambda = -\xi\omega_n^\alpha + i\omega_n^\alpha\sqrt{1-\xi^2}$, the system eigenvalue could be determined by the damping coefficient ξ and natural frequency ω_n [33]. In general, design specifications are often given in terms of $\xi_{\min}$ and ω_n. Define $\eta = \arccos(\xi_{\min}), \rho = \omega_n^\alpha$, and we can determine a circle region $S(0, r)$ with the center being the coordinate origin, the radius being r [34], and

$$r = \rho/\sin(\eta). \tag{2.5}$$

If $\lambda \in S(0, r) \cap \mathscr{D}_s$, it implies that the eigenvalue is stable. Hence, in this restrained stability region, we choose n circle regions with different radii to complete multiple-region eigenvalue assignment, as shown in Figure 3.

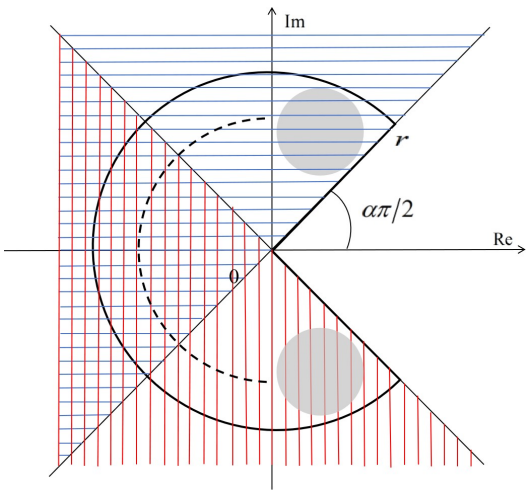

Figure 3. n circle eigenvalue assignment regions.

Note that circle region can be described by the GLMI form, and let the center of the k-th circle region be (a_k, b_k) and the radius be r_k, where $a_k^2 + b_k^2 - r_k^2 > 0$, then the k-th circle region is described by

$$\mathscr{D}_{R_k} = \left\{ s_k \in \mathbb{C} : f_{\mathscr{D}_{R_k}}(s_k) = H_{k1} + s_k H_{k2} + \bar{s}_k H_{k2}^H + s_k \bar{s}_k H_{k3} < 0 \right\}, \tag{2.6}$$

where $H_{k1} = a_k^2 + b_k^2 - r_k^2, H_{k2} = -(a_k - ib_k), H_{k3} = 1$. While the set of eigenvalues is self-conjugate, the conjugate eigenvalues should be located in two circle regions, which are symmetric about the real axis. That is to say that the corresponding symmetric circle region to $\mathscr{D}_{R_k}$ can be described as

$$\mathscr{D}_{R_{n-k}} = \left\{ s_k \in \mathbb{C} : f_{\mathscr{D}_{R_{n-k}}}(s_k) = \left(a_k^2 + b_k^2 - r_k^2\right) + s_k(a_k + ib_k) - \bar{s}_k(a_k - ib_k) + s_k\bar{s}_k < 0 \right\}. \tag{2.7}$$

Subsequently, we present the following definition of MGLMI regions:

Definition 2.2. *$\mathscr{D}_U$ is defined as the set consisting of n GLMI regions*

$$\mathscr{D}_U = \bigcup_{k=1}^{n} \mathscr{D}_{R_k}, \tag{2.8}$$

where $\mathscr{D}_{R_k}$ is the k-th GLMI region determined by (2.6). Let $H_1 = diag\{H_{11}, \ldots, H_{n1}\} \in \mathbb{C}^{n\times n}$, $H_2 = diag\{H_{12}, \ldots, H_{n2}\} \in \mathbb{C}^{n\times n}$, and $H_3 = diag\{H_{13}, \ldots, H_{n3}\} \in \mathbb{C}^{n\times n}$. If the variable $s \in \mathbb{C}$ is in $\mathscr{D}_U$, then $\mathscr{D}_U$ can be described as

$$f_{\mathscr{D}_U}(s) = H_1 + sH_2 + \bar{s}H_2^H + s\bar{s}H_3 < 0, \tag{2.9}$$

where $f_{\mathscr{D}_U}(s)$ is the characteristic function of $\mathscr{D}_U$.

Based on the above analysis, the selection criteria for fractional-order multiple stability regions is to first define a restrained sector region with the center as the coordinate origin and the radius r according to the minimum damping coefficient $\xi_{\min}$ and natural frequency ω_n. Then, we choose n circle regions $\mathscr{D}_U$ defined by Definition 2.2. Therefore, solving **Problem MREAP** is to find F such that all the eigenvalues of $A + BF$ are in the MGLMI regions $\mathscr{D}_U$.

3. Solutions to problem MREAP

In this section, we first provide the equivalent condition for all the eigenvalues of A to be in the MGLMI regions $\mathscr{D}_U$.

Theorem 3.1. *All the eigenvalues of $A \in \mathbb{R}^{n\times n}$ are in the MGLMI regions $\mathscr{D}_U$ if and only if there exists a symmetric positive definite matrix $P \in \mathbb{R}^{n\times n}$ satisfying*

$$M_{\mathscr{D}_U}(A, P) < 0, \tag{3.1}$$

where

$$M_{\mathscr{D}_U}(A, P) = H_1 \otimes P + H_2 \otimes AP + H_2^H \otimes PA^H + H_3 \otimes APA^H. \tag{3.2}$$

Proof. **(Sufficiency)** Assume that the condition (3.1) holds. Let λ_l be an arbitrary eigenvalue of A and $v_l \in \mathbb{C}^n$ the corresponding eigenvector, which means that $v_l^H A = \lambda_l v_l^H$. This yields

$$\begin{aligned}
&\left(I_n \otimes v_l^H\right) M_{\mathscr{D}_U}(A, P)\left(I_n \otimes v_l\right) \\
&= \left(I_n \otimes v_l^H\right)\left(H_1 \otimes P + H_2 \otimes AP + H_2^H \otimes PA^H + H_3 \otimes APA^H\right)\left(I_n \otimes v_l\right) \\
&= H_1 \otimes \left(v_l^H P v_l\right) + H_2 \otimes \left(v_l^H A P v_l\right) + H_2^H \otimes \left(v_l^H P A^H v_l\right) + H_3 \otimes \left(v_l^H A P A^H v_l\right) \\
&= \left(v_l^H P v_l\right)\left(H_1 + \lambda_l H_2 + \bar{\lambda}_l H_2^H + \lambda_l \bar{\lambda}_l H_3\right).
\end{aligned} \tag{3.3}$$

If (3.1) holds and $P > 0$, (3.3) implies that

$$H_1 + \lambda_l H_2 + \bar{\lambda}_l H_2^H + \lambda_l \bar{\lambda}_l H_3 < 0, \tag{3.4}$$

which means that the arbitrary eigenvalue $\lambda_l\,(l = 1, \ldots, n)$ is distributed in $\mathscr{D}_U$.

(Necessity) Suppose that all eigenvalues of A are in the MGLMI regions; we need to find $P = P^T > 0$ satisfying (3.1). We first consider the case where A is diagonalizable. Then, there exists a nonsingular

matrix $V \in \mathbb{C}^{n\times n}$ satisfying $V^{-1}AV = \Lambda = diag\{\lambda_1, \ldots, \lambda_n\}$, where $\lambda_l (l = 1, \ldots, n) \in \mathscr{D}_U$. It can be verified that

$$\begin{aligned} & M_{\mathscr{D}_U}(\Lambda, I_n) \\ &= H_1 \otimes I_n + H_2 \otimes \Lambda + H_2^H \otimes \Lambda^H + H_3 \otimes \Lambda\Lambda^H \\ &= W^H diag\{f_{\mathscr{D}_U}(\lambda_1), \ldots, f_{\mathscr{D}_U}(\lambda_n)\} W, \end{aligned} \tag{3.5}$$

where W is a elementary transformation matrix. Since $\lambda_l \in \mathscr{D}_U$, it follows that $f_{\mathscr{D}_U}(\lambda_l) < 0$. Hence, we have $M_{\mathscr{D}_U}(\Lambda, I_n) < 0$. Then, pre- and post-multiplying $M_{\mathscr{D}_U}(\Lambda, I_n)$ by $(I_n \otimes V)$ and $\left(I_n \otimes V^H\right)$, respectively, it yields

$$\begin{aligned} & (I_n \otimes V) M_{\mathscr{D}_U}(\Lambda, I_n) \left(I_n \otimes V^H\right) \\ &= (I_n \otimes V)\left(H_1 \otimes I_n + H_2 \otimes \Lambda + H_2^H \otimes \Lambda^H + H_3 \otimes \Lambda\Lambda^H\right)\left(I_n \otimes V^H\right) \\ &= H_1 \otimes \left(VV^H\right) + H_2 \otimes \left(V\Lambda V^H\right) + H_2^H \otimes \left(V\Lambda^H V^H\right) + H_3 \otimes \left(V\Lambda\Lambda^H V^H\right) \\ &= H_1 \otimes \left(VV^H\right) + H_2 \otimes \left(AVV^H\right) + H_2^H \otimes \left(VV^H A^H\right) + H_3 \otimes \left(AVV^H A^H\right) \\ &= M_{\mathscr{D}_U}\left(A, VV^H\right). \end{aligned} \tag{3.6}$$

It means that there exists $P = VV^H > 0$ satisfying $M_{\mathscr{D}_U}(A, P) < 0$.

In the case where A is not-diagonalizable, there exists a nonsingular matrix $V \in \mathbb{C}^{n\times n}$ satisfying $V^{-1}AV = J = diag\{J_1, \ldots, J_s\}$, where $J_r (r = 1, \ldots, s)$ is the Jordan block,

$$J_r = \begin{bmatrix} \lambda_r & 1 & & & \\ & \lambda_r & 1 & & \\ & & \ddots & \ddots & \\ & & & \lambda_r & 1 \\ & & & & \lambda_r \end{bmatrix}_{n_r \times n_r}, \lambda_r \in \mathscr{D}_U, \sum_{r=1}^{s} n_r = n. \tag{3.7}$$

Assuming that

$$\Lambda = \begin{bmatrix} \lambda_1 I_{n_1} & & & \\ & \ddots & & \\ & & \lambda_{s-1} I_{n_{s-1}} & \\ & & & \lambda_s I_{n_s} \end{bmatrix}, \tag{3.8}$$

one can construct a sequence of invertible matrices T_k such that

$$\lim_{k\to\infty} T_k^{-1} J T_k = \lim_{k\to\infty} diag\{\Lambda_1, \ldots, \Lambda_s\} = diag\{\lambda_1 I_{n_1}, \ldots, \lambda_s I_{n_s}\} = \Lambda. \tag{3.9}$$

Based on the above analysis, we have $M_{\mathscr{D}_U}(\Lambda, I_n) < 0$, then

$$\lim_{k\to\infty} M_{\mathscr{D}_U}\left(T_k^{-1} J T_k, I_n\right) < 0. \tag{3.10}$$

Then, k is sufficient large, which satisfies $M_{\mathscr{D}_U}\left(T_k^{-1} J T_k, I_n\right) < 0$. Together with $J = V^{-1}AV$, let $T = T_k$, then we can obtain $M_{\mathscr{D}_U}\left(T^{-1}V^{-1}AVT, I_n\right) < 0$. Pre- and post-multiplying $M_{\mathscr{D}_U}\left(T^{-1}V^{-1}AVT, I_n\right)$ by

$(I_n \otimes TV)$ and $\left(I_n \otimes V^H T^H\right)$, respectively, yields

$$\begin{aligned}
&(I_n \otimes TV)\, M_{\mathscr{D}_U}\left(T^{-1}V^{-1}AVT, I_n\right)\left(I \otimes V^H T^H\right) \\
&= (I_n \otimes TV)\begin{pmatrix} H_1 \otimes I_n + H_2 \otimes \left(T^{-1}V^{-1}AVT\right) \\ +H_2^H \otimes \left(T^{-1}V^{-1}AVT\right)^H \\ +H_3 \otimes \left(T^{-1}V^{-1}AVT\right)\left(T^{-1}V^{-1}AVT\right)^H \end{pmatrix}\left(I_n \otimes V^H T^H\right) \\
&= H_1 \otimes \left(TVV^H T^H\right) + H_2 \otimes \left(ATVV^H T^H\right) + H_2^H \otimes \left(TVT^H V^H A^H\right) + H_3 \otimes \left(ATVV^H T^H A^H\right) \\
&= M_{\mathscr{D}_U}\left(A, TVV^H T^H\right) < 0.
\end{aligned} \tag{3.11}$$

Since T and V are invertible matrices, $P = TVV^H T^H$ is positive definite. This implies that there exists $P > 0$ satisfying $M_{\mathscr{D}_U}(A, P) < 0$.

We observe that $P = P^H > 0$ is not necessarily a real matrix. Set $P = P_1 + iP_2$, where $P_1 = \mathrm{Re}(P)$ and $P_2 = \mathrm{Im}(P)$ denote the real and imaginary part of P, respectively, then $P_1 = P_1^T > 0$. For the matrix A, we have

$$\begin{aligned}
&M_{\mathscr{D}_U}(A, P) \\
&= H_1 \otimes (P_1 + iP_2) + H_2 \otimes A(P_1 + iP_2) + H_2^H \otimes (P_1 + iP_2)A^H + H_3 \otimes A(P_1 + iP_2)A^H \\
&= \left[H_1 \otimes P_1 + H_2 \otimes AP_1 + H_2^H \otimes P_1 A^H + H_3 \otimes AP_1 A^H\right] \\
&\quad + i\left[H_1 \otimes P_2 + H_2 \otimes AP_2 + H_2^H \otimes P_2 A^H + H_3 \otimes AP_2 A^H\right] \\
&\triangleq M_{\mathscr{D}_U}(A, P_1) + iM_{\mathscr{D}_U}(A, P_2),
\end{aligned} \tag{3.12}$$

where we can verify that $M_{\mathscr{D}_U}(A, P_1) = \left(M_{\mathscr{D}_U}(A, P_1)\right)^H$ and $M_{\mathscr{D}_U}(A, P_2) = -\left(M_{\mathscr{D}_U}(A, P_2)\right)^H$ according to $H_1 = H_1^H$ and $H_3 = H_3^H$. Therefore, for any non-zero vector $y \in \mathbb{C}^{n^2}$, we have $y^H M_{\mathscr{D}_U}(A, P_2)\, y = 0$. According to (3.12), we know that $y^H M_{\mathscr{D}_U}(A, P)\, y = y^H M_{\mathscr{D}_U}(A, P_1)\, y$. Since $M_{\mathscr{D}_U}(A, P) < 0$, it implies that $M_{\mathscr{D}_U}(A, P_1) < 0$, where P_1 is the required symmetric positive definite matrix.

Since the condition in Theorem 3.1 involves complex matrices H_1, H_2, and H_3, we propose the following theorem to avoid the use of complex matrices that are incompatible with the LMI toolbox in MATLAB.

Theorem 3.2. *Let H_{kR} and H_{kI} be the real part and the imaginary part, respectively, of $H_k, k = 1, 2, 3$, and we denote*

$$\begin{aligned}
\tilde{H}_1 &= \begin{bmatrix} H_{1R} + iH_{1I} & \\ & H_{1R} - iH_{1I} \end{bmatrix}, \\
\tilde{H}_2 &= \begin{bmatrix} H_{2R} + iH_{2I} & \\ & H_{2R} - iH_{2I} \end{bmatrix}, \\
\tilde{H}_3 &= \begin{bmatrix} H_{3R} + iH_{3I} & \\ & H_{3R} - iH_{3I} \end{bmatrix}.
\end{aligned} \tag{3.13}$$

Then

$$\hat{H}_1 \otimes P + \hat{H}_2 \otimes AP + \hat{H}_2^H \otimes PA^H + \hat{H}_3 \otimes APA^H < 0, \tag{3.14}$$

where

$$\hat{H}_1 = \begin{bmatrix} H_{1R} & H_{1I} \\ -H_{1I} & H_{1R} \end{bmatrix}, \hat{H}_2 = \begin{bmatrix} H_{2R} & H_{2I} \\ -H_{2I} & H_{2R} \end{bmatrix}, \hat{H}_3 = \begin{bmatrix} H_{3R} & H_{3I} \\ -H_{3I} & H_{3R} \end{bmatrix}, \tag{3.15}$$

if and only if

$$\tilde{H}_1 \otimes P + \tilde{H}_2 \otimes AP + \tilde{H}_2^H \otimes PA^H + \tilde{H}_3 \otimes APA^H < 0, \tag{3.16}$$

which implies that all the eigenvalues of A are in the MGLMI regions $\mathscr{D}_U$ with complex matrices H_1, H_2, H_3.

Proof. Let

$$\mathrm{N} = \frac{1}{\sqrt{2}} \begin{bmatrix} I_n & I_n \\ iI_n & -iI_n \end{bmatrix}, \tag{3.17}$$

then we can get

$$\begin{aligned} \mathrm{N}\tilde{H}_1\mathrm{N}^H &= \tfrac{1}{2} \begin{bmatrix} I_n & I_n \\ iI_n & -iI_n \end{bmatrix} \begin{bmatrix} H_{1R} + iH_{1I} & \\ & H_{1R} - iH_{1I} \end{bmatrix} \begin{bmatrix} I_n & I_n \\ iI_n & -iI_n \end{bmatrix}^H \\ &= \begin{bmatrix} H_{1R} & H_{1I} \\ -H_{1I} & H_{1R} \end{bmatrix} \\ &= \hat{H}_1. \end{aligned} \tag{3.18}$$

Similarly, it also has

$$\mathrm{N}\tilde{H}_2\mathrm{N}^H = \hat{H}_2, \mathrm{N}\tilde{H}_3\mathrm{N}^H = \hat{H}_3. \tag{3.19}$$

Then it follows that

$$\begin{aligned} &\hat{H}_1 \otimes P + \hat{H}_2 \otimes AP + \hat{H}_2^H \otimes PA^H + \hat{H}_3 \otimes APA^H \\ &= \mathrm{N}\tilde{H}_1\mathrm{N}^H \otimes P + \mathrm{N}\tilde{H}_2\mathrm{N}^H \otimes AP + \mathrm{N}\tilde{H}_2^H\mathrm{N}^H \otimes PA^H + \mathrm{N}\tilde{H}_3\mathrm{N}^H \otimes APA^H \\ &= (\mathrm{N} \otimes I_n)\left(\tilde{H}_1 \otimes P + \tilde{H}_2 \otimes AP + \tilde{H}_2^H \otimes PA^H + \tilde{H}_3 \otimes APA^H\right)\left(\mathrm{N}^H \otimes I_n\right). \end{aligned} \tag{3.20}$$

If (3.14) holds, it is deduced that $\tilde{H}_1 \otimes P + \tilde{H}_2 \otimes AP + \tilde{H}_2^H \otimes PA^H + \tilde{H}_3 \otimes APA^H < 0$. It can be obtained that all the eigenvalues of A are in the MGLMI regions, which consist of complex matrices H_1, H_2, H_3. Conversely, (3.14) can be derived from (3.16) in a similar way.

Before solving the matrix F, we define the closed-loop system matrix as $A_c = A + BF$. Based on Theorem 3.2, all the eigenvalues of A_c are in the MGLMI regions $\mathscr{D}_U$ if and only if (3.14) holds for A_c. Hence, we have

$$\hat{H}_1 \otimes P + \hat{H}_2 \otimes A_cP + \hat{H}_2^H \otimes PA_c^H + \hat{H}_3 \otimes A_cPA_c^H < 0, \tag{3.21}$$

which can be reorganized as

$$\hat{H}_1 \otimes P + \hat{H}_2 \otimes (A + BF)\, P + \hat{H}_2^H \otimes P(A + BF)^H + \hat{H}_3 \otimes (A + BF)\, P(A + BF)^H < 0. \tag{3.22}$$

From (3.22), we know that the matrices P and F are unknown, which implies that (3.22) has nonlinear terms of the unknowns. Hence, we give a sufficient condition for solving the feedback control matrix F.

Theorem 3.3. *For the given fractional-order system (1.1), the MGLMI regions $\mathscr{D}_U$ with the given matrices $\hat{H}_k\,(k = 1, 2, 3)$ are defined by (3.15), if there exist $M \in \mathbb{R}^{n\times n}$, $S \in \mathbb{R}^{l\times n}$, and a symmetric positive definite matrix $P \in \mathbb{R}^{n\times n}$ satisfying*

$$\Omega = \begin{bmatrix} \Omega_1 & \Omega_2 \\ \Omega_2^H & \Omega_3 \end{bmatrix} < 0, \tag{3.23}$$

where

$$\Omega_k = \begin{bmatrix} \Omega_{k1} & \Omega_{k2} \\ \Omega_{k3} & \Omega_{k4} \end{bmatrix}, k = 1, 2, 3, \tag{3.24}$$

and

$$\begin{aligned}
\Omega_{11} &= H_{1R} \otimes P + H_{2R} \otimes (AM + BS) + H_{2R}^H \otimes (AM + BS)^H, \\
\Omega_{12} &= H_{1I} \otimes P + H_{2I} \otimes (AM + BS) - H_{2I}^H \otimes (AM + BS)^H, \\
\Omega_{13} &= -H_{1I} \otimes P - H_{2I} \otimes (AM + BS) + H_{2I}^H \otimes (AM + BS)^H, \\
\Omega_{14} &= H_{1R} \otimes P + H_{2R} \otimes (AM + BS) + H_{2R}^H \otimes (AM + BS)^H, \\
\Omega_{21} &= H_{2R}^H \otimes \left(P - M^H\right) + H_{3R} \otimes (AM + BS), \\
\Omega_{22} &= -H_{2I}^H \otimes \left(P - M^H\right) + H_{3I} \otimes (AM + BS), \\
\Omega_{23} &= H_{2I}^H \otimes \left(P - M^H\right) - H_{3I} \otimes (AM + BS), \\
\Omega_{24} &= H_{2R}^H \otimes \left(P - M^H\right) + H_{3R} \otimes (AM + BS), \\
\Omega_{31} &= H_{3R} \otimes P - H_{3R} \otimes M - H_{3R} \otimes M^H, \\
\Omega_{32} &= H_{3I} \otimes P - H_{3I} \otimes M - H_{3I} \otimes M^H, \\
\Omega_{33} &= -H_{3I} \otimes P + H_{3I} \otimes M + H_{3I} \otimes M^H, \\
\Omega_{34} &= H_{3R} \otimes P - H_{3R} \otimes M - H_{3R} \otimes M^H,
\end{aligned} \tag{3.25}$$

then all the eigenvalues of $A + BF$ are in the MGLMI regions $\mathscr{D}_U$, and M is a nonsingular matrix such that the feedback control matrix is

$$F = S M^{-1}. \tag{3.26}$$

Proof. We first prove that the matrix M is nonsingular. Based on the selection criteria for fractional-order multiple stability regions, we know that $H_{k1} = a_k^2 + b_k^2 - r_k^2$ and $H_{k3} = 1$ $(k = 1, \ldots, n)$. According to Definition 2.2, it yields that

$$\begin{aligned}
H_1 &= diag\{H_{11}, \ldots, H_{n1}\} = diag\left\{a_1^2 + b_1^2 - r_1^2, \ldots, a_n^2 + b_n^2 - r_n^2\right\}, \\
H_3 &= diag\{H_{13}, \ldots, H_{n3}\} = diag\{1, \ldots, 1\}.
\end{aligned} \tag{3.27}$$

Thus, we have $H_1 = H_1^H, H_3 = H_3^H$. Combined with $\hat{H}_k$ $(k = 1, 2, 3)$ defined by (3.15), we can get

$$\begin{aligned}
H_{1R} &= diag\left\{a_1^2 + b_1^2 - r_1^2, \ldots, a_n^2 + b_n^2 - r_n^2\right\}, H_{1I} = diag\{0, \ldots, 0\}, \\
H_{3R} &= diag\{1, \ldots, 1\}, H_{3I} = diag\{0, \ldots, 0\}.
\end{aligned} \tag{3.28}$$

Therefore, $\hat{H}_1 = \hat{H}_1^H$, $\hat{H}_3 = \hat{H}_3^H = I_{n^2} > 0$. Set $M = FS$ and $A_c = A + BF$, then $\Omega_1, \Omega_2, \Omega_3$ can be briefly written as

$$\begin{aligned}
\Omega_1 &= \hat{H}_1 \otimes P + \hat{H}_2 \otimes A_c M + \hat{H}_2^H \otimes (A_c M)^H, \\
\Omega_2 &= \hat{H}_2^H \otimes \left(P - M^H\right) + \hat{H}_3 \otimes A_c M, \\
\Omega_3 &= \hat{H}_3 \otimes \left(P - M - M^H\right).
\end{aligned} \tag{3.29}$$

It can be verified that $\Omega_1 = \Omega_1^H$ and $\Omega_3 = \Omega_3^H$ because P is symmetric positive definite. Furthermore, we have $\Omega = \begin{bmatrix} \Omega_1 & \Omega_2 \\ \Omega_2^H & \Omega_3 \end{bmatrix} = \Omega^H$. Since $\Omega < 0$, it is equivalent to $\Omega_3 < 0$ [34], that is, $\Omega_3 = \hat{H}_3 \otimes \left(P - M - M^H\right) < 0$. Based on the above analysis, we have $\hat{H}_3 = \hat{H}_3^H > 0$ and $P > 0$, and it can be verified that $M + M^H > P > 0$. Thus $M + M^H > 0$. Since $M \in \mathbb{R}^{n \times n}$, it yields that $M^H = M^T, M + M^T = \left(M + M^T\right)^T > 0$. Then for any non-zero vector $x \in \mathbb{R}^n$, there is $x^T \left(M + M^T\right) x > 0$. Let λ be an arbitrary eigenvalue of M and x be the corresponding eigenvector, and it can be verified that $x^T \left(M + M^T\right) x = x^T M x + x^T M^T x = 2\lambda x^T x > 0$. Therefore, $\lambda > 0$ for $x \neq 0$, then M is nonsingular.

Next, we prove that all the eigenvalues of $A + BF$ are in the MGLMI regions. Based on the above analysis, (3.23) can be rewritten as

$$\begin{bmatrix} \hat{H}_1 \otimes P + \hat{H}_2 \otimes A_c M + \hat{H}_2^H \otimes (A_c M)^H & \hat{H}_2^H \otimes \left(P - M^H\right) + \hat{H}_3 \otimes A_c M \\ \hat{H}_2 \otimes (P - M) + \hat{H}_3 \otimes (A_c M)^H & \hat{H}_3 \otimes \left(P - M - M^H\right) \end{bmatrix} < 0. \tag{3.30}$$

Let $T = [I \quad I \otimes A_c]^T$, and pre- and post-multiplying (3.30) by T^T and T, respectively, we deduce

$$\begin{aligned} &T^T \begin{bmatrix} \hat{H}_1 \otimes P + \hat{H}_2 \otimes A_c M + \hat{H}_2^H \otimes (A_c M)^H & \hat{H}_2^H \otimes \left(P - M^H\right) + \hat{H}_3 \otimes A_c M \\ \hat{H}_2 \otimes (P - M) + \hat{H}_3 \otimes (A_c M)^H & \hat{H}_3 \otimes \left(P - M - M^H\right) \end{bmatrix} T \\ &= \hat{H}_1 \otimes P + \hat{H}_2 \otimes A_c P + \hat{H}_2^H \otimes P A_c^H + \hat{H}_3 \otimes A_c P A_c^H < 0. \end{aligned} \tag{3.31}$$

This means that if there exist matrices P, M, S such that $\Omega < 0$, we can reduce that $\hat{H}_1 \otimes P + \hat{H}_2 \otimes A_c P + \hat{H}_2^H \otimes P A_c^H + \hat{H}_3 \otimes A_c P A_c^H < 0$. According to Theorems 3.1 and 3.2, it means that all the eigenvalues of $A + BF$ are in the MGLMI regions $\mathscr{D}_U$.

Furthermore, we give the expression of F. By solving the matrix inequality (3.23), we can obtain S and M. Since M is nonsingular and $M = FS$, we can get the feedback control matrix $F = SM^{-1}$.

Based on the above analysis, we present a numerical algorithm for solving active vibration control for fractional-order systems based on multiple-region eigenvalue assignment.

Algorithm 1 Multiple-region eigenvalue assignment algorithm

Input: $A, B, \alpha, \xi_{\min}, \omega_n, a_k, b_k$ and $r_k, k = 1, \ldots, n$.

Output: The feedback control matrix F.

1: Compute $\eta = \arccos(\xi_{\min}), \rho = \omega_n^\alpha$;

2: Compute radius

$$r = \rho / \sin(\eta);$$

3: Compute the matrices

$$\begin{aligned} H_{k1} &= a_k^2 + b_k^2 - r_k^2, \\ H_{k2} &= -(a_k - ib_k), \\ H_{k3} &= 1, k = 1, \ldots, n; \end{aligned}$$

4: Form the matrices $H_1 = diag\{H_{11}, \ldots, H_{n1}\}, H_2 = diag\{H_{12}, \ldots, H_{n2}\}, H_3 = diag\{H_{13}, \ldots, H_{n3}\}$;

5: Separate the real part $H_{kR}\,(k = 1, 2, 3)$ and the imaginary part $H_{kI}\,(k = 1, 2, 3)$ of the matrices H_1, H_2, H_3;

6: Select the matrices P, M, S;

7: Compute the matrices $\Omega_{kj}\,(k = 1, 2, 3, j = 1, 2, 3, 4)$ by (3.25);

8: Form the matrices $\Omega_k = \begin{bmatrix} \Omega_{k1} & \Omega_{k2} \\ \Omega_{k3} & \Omega_{k4} \end{bmatrix} (k = 1, 2, 3)$ and $\Omega = \begin{bmatrix} \Omega_1 & \Omega_2 \\ \Omega_2^H & \Omega_3 \end{bmatrix}$;

9: Solve the matrix inequality $\Omega < 0$ for the matrices M and S;

10: Compute the feedback control matrix $F = SM^{-1}$.

4. Numerical examples

In Section 4, the feasibility of our algorithm is demonstrated through numerical examples of fractional-order quadrotor UAV systems, electrical circuit systems, and rotary inverted pendulum

systems. In Section 4.1, we present the mathematical modeling of a fractional-order quadrotor UAV system and verify the validity of the multiple-region eigenvalue assignment method and the stability of the flight systems. In Section 4.2, we provide the experimental results of this approach combined with fractional-order electrical circuit systems, which indicate that the system stability and region constraint requirements are achieved. In Section 4.3, we compare single-region eigenvalue assignment with our method through an experiment on a fractional-order rotary inverted pendulum system. The results imply that the multiple-region eigenvalue assignment method improves system performance.

4.1. Fractional-order quadrotor UAV systems

Existing research has confirmed that the metal materials of the shell, the damping materials of the wings, and the mechanical stresses in the physical structure of quadrotor UAV all exhibit fractional-order characteristics [35]. Additionally, the motor subsystem, responsible for propeller rotation to generate propulsion, the battery subsystem that provides endurance energy, and the speed control subsystem have also been confirmed to exhibit fractional-order features [36, 37]. Therefore, the quadrotor UAV system should fundamentally be considered as a fractional-order system, as shown in Figure 4 [38, 39]. The dynamic model of quadrotor UAV system is given in [40].

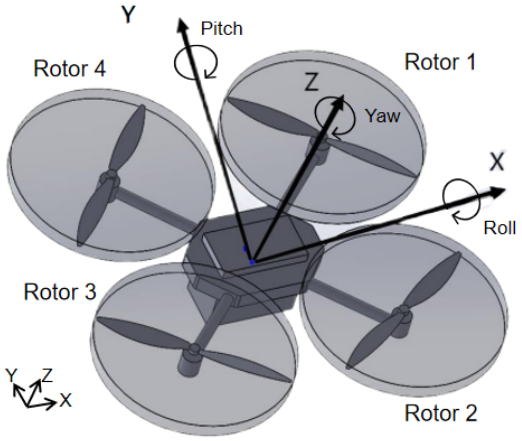

Figure 4. Model of the quadrotor UAV.

$$\begin{cases} \ddot{x} = (\sin\theta\cos\varphi\cos\psi + \sin\varphi\sin\psi)\,\frac{U_1}{m} - \frac{K_1}{m}\dot{x}, \\ \ddot{y} = (\sin\theta\cos\varphi\sin\psi - \sin\varphi\cos\psi)\,\frac{U_1}{m} - \frac{K_2}{m}\dot{y}, \\ \ddot{z} = (\cos\theta\cos\varphi)\,\frac{U_1}{m} - \frac{K_3}{m}\dot{z} - g, \\ \ddot{\varphi} = \frac{U_2}{I_x} + \frac{I_y - I_z}{I_x}\dot{\psi}\dot{\theta} - \frac{J_r}{I_x}\Omega_r\dot{\theta} - \frac{lK_4}{I_x}\dot{\varphi}, \\ \ddot{\theta} = \frac{U_3}{I_y} + \frac{I_z - I_x}{I_y}\dot{\psi}\dot{\varphi} - \frac{J_r}{I_y}\Omega_r\dot{\varphi} - \frac{lK_5}{I_y}\dot{\theta}, \\ \ddot{\psi} = \frac{U_4}{I_z} + \frac{I_x - I_y}{I_z}\dot{\varphi}\dot{\theta} - \frac{lK_6}{I_z}\dot{\psi}, \end{cases} \tag{4.1}$$

where x, y, z are the position of the center of mass, φ, θ, ψ are the roll, pitch, and yaw angle of the quadrotor, I_x, I_y, I_z are the moments of inertia, J_r and Ω_r are the principle moments of inertia and angular velocity, m is the total mass, g is the gravitational acceleration, l is the distance from the rotor to the center of mass, K_i $(i = 1, \ldots, 6)$ is the drag coefficient, and U_1, U_2, U_3, U_4 are the total, roll, pitch, and yaw forces.

In general applications, we assume that the quadrotor UAV works in a hovering condition, which implies that $U_1 \approx mg$. Also, the drag coefficients for the system and the influence of four propellers on the gyroscopic torque of the aircraft can be neglected, which means that $J_r = 0, K_i = 0, i = 1, \ldots, 6$. In addition, the pitch and roll angles are so small that $\cos\theta \approx 1, \sin\theta \approx \theta, \cos\varphi \approx 1, \sin\varphi \approx \varphi$. The yaw angle is close to zero, and we have $\cos\psi \approx 1, \sin\psi \approx 0$. Then, (4.1) can be simply written as

$$\begin{cases} \ddot{x} = g\theta, \\ \ddot{y} = -g\varphi, \\ \ddot{z} = \frac{U_1}{m}, \\ \ddot{\varphi} = \frac{U_2}{I_x}, \\ \ddot{\theta} = \frac{U_3}{I_y}, \\ \ddot{\psi} = \frac{U_4}{I_z}. \end{cases} \tag{4.2}$$

Based on the analysis mentioned earlier, we introduce the fractional-order derivative in (4.2), and the state variables will be assumed as follows:

$$\begin{cases} x_1 = x, \\ x_2 = D^{0.5}x, \\ x_3 = \dot{x}, \\ x_4 = D^{1.5}x, \end{cases} \begin{cases} x_5 = y, \\ x_6 = D^{0.5}y, \\ x_7 = \dot{y}, \\ x_8 = D^{1.5}y, \end{cases} \begin{cases} x_9 = z, \\ x_{10} = D^{0.5}z, \\ x_{11} = \dot{z}, \\ x_{12} = D^{1.5}z, \end{cases} \begin{cases} x_{13} = \varphi, \\ x_{14} = D^{0.5}\varphi, \\ x_{15} = \dot{\varphi}, \\ x_{16} = D^{1.5}\varphi, \end{cases} \begin{cases} x_{17} = \theta, \\ x_{18} = D^{0.5}\theta, \\ x_{19} = \dot{\theta}, \\ x_{20} = D^{1.5}\theta, \end{cases} \begin{cases} x_{21} = \psi, \\ x_{22} = D^{0.5}\psi, \\ x_{23} = \dot{\psi}, \\ x_{24} = D^{1.5}\psi. \end{cases} \tag{4.3}$$

Therefore, model (4.2) can be transformed into the fractional-order linear control system with fractional order $\alpha = 0.5$ in the following representation

$$D^{0.5}\begin{pmatrix} x_1 \\ x_2 \\ \vdots \\ x_{24} \end{pmatrix} = \begin{bmatrix} A_1 & \mathbf{0} & \mathbf{0} & \mathbf{0} & A_7 & \mathbf{0} \\ \mathbf{0} & A_2 & \mathbf{0} & \mathbf{0} & \mathbf{0} & \mathbf{0} \\ \mathbf{0} & \mathbf{0} & A_3 & A_8 & \mathbf{0} & \mathbf{0} \\ \mathbf{0} & \mathbf{0} & \mathbf{0} & A_4 & \mathbf{0} & \mathbf{0} \\ \mathbf{0} & \mathbf{0} & \mathbf{0} & \mathbf{0} & A_5 & \mathbf{0} \\ \mathbf{0} & \mathbf{0} & \mathbf{0} & \mathbf{0} & \mathbf{0} & A_6 \end{bmatrix}\begin{pmatrix} x_1 \\ x_2 \\ \vdots \\ x_{24} \end{pmatrix} + \begin{bmatrix} \mathbf{0} \\ \mathbf{0} \\ B_1 \\ B_2 \\ B_3 \\ B_4 \end{bmatrix}\begin{pmatrix} U_1 \\ U_2 \\ U_3 \\ U_4 \end{pmatrix}, \tag{4.4}$$

where $\mathbf{0}$ is the zero matrix of order 4, and

$$A_i = \begin{bmatrix} 0 & 1 & 0 & 0 \\ 0 & 0 & 1 & 0 \\ 0 & 0 & 0 & 1 \\ 0 & 0 & 0 & 0 \end{bmatrix}, i = 1, \ldots, 6,$$

$$A_7 = \begin{bmatrix} 0 & 0 & 0 & 0 \\ 0 & 0 & 0 & 0 \\ 0 & 0 & 0 & 0 \\ g & 0 & 0 & 0 \end{bmatrix}, A_8 = \begin{bmatrix} 0 & 0 & 0 & 0 \\ 0 & 0 & 0 & 0 \\ 0 & 0 & 0 & 0 \\ -g & 0 & 0 & 0 \end{bmatrix},$$

$$B_1 = \begin{bmatrix} 0 & 0 & 0 & 0 \\ 0 & 0 & 0 & 0 \\ 0 & 0 & 0 & 0 \\ 1/m & 0 & 0 & 0 \end{bmatrix}, B_2 = \begin{bmatrix} 0 & 0 & 0 & 0 \\ 0 & 0 & 0 & 0 \\ 0 & 0 & 0 & 0 \\ 0 & 1/I_x & 0 & 0 \end{bmatrix},$$

$$B_3 = \begin{bmatrix} 0 & 0 & 0 & 0 \\ 0 & 0 & 0 & 0 \\ 0 & 0 & 0 & 0 \\ 0 & 0 & 1/I_y & 0 \end{bmatrix}, B_4 = \begin{bmatrix} 0 & 0 & 0 & 0 \\ 0 & 0 & 0 & 0 \\ 0 & 0 & 0 & 0 \\ 0 & 0 & 0 & 1/I_z \end{bmatrix}.$$

Namely, we have

$$D^{\alpha} x(t) = Ax(t) + Bu(t), \tag{4.5}$$

where $x(t) = [x_1, \ldots, x_{24}]^T \in \mathbb{R}^{24}$, $u(t) = [U_1, U_2, U_3, U_4]^T \in \mathbb{R}^4$, the fractional order $\alpha = 0.5$, and the system matrices $A \in \mathbb{R}^{24\times 24}$ and $B \in \mathbb{R}^{24\times 4}$ are, respectively,

$$A = \begin{bmatrix} A_1 & \mathbf{0} & \mathbf{0} & \mathbf{0} & A_7 & \mathbf{0} \\ \mathbf{0} & A_2 & \mathbf{0} & \mathbf{0} & \mathbf{0} & \mathbf{0} \\ \mathbf{0} & \mathbf{0} & A_3 & A_8 & \mathbf{0} & \mathbf{0} \\ \mathbf{0} & \mathbf{0} & \mathbf{0} & A_4 & \mathbf{0} & \mathbf{0} \\ \mathbf{0} & \mathbf{0} & \mathbf{0} & \mathbf{0} & A_5 & \mathbf{0} \\ \mathbf{0} & \mathbf{0} & \mathbf{0} & \mathbf{0} & \mathbf{0} & A_6 \end{bmatrix}, B = \begin{bmatrix} \mathbf{0} \\ \mathbf{0} \\ B_1 \\ B_2 \\ B_3 \\ B_4 \end{bmatrix}.$$

Since the fractional-order model can be separately developed for each channel of the quadrotor UAV system, we perform the experimental results in yaw and x-axis channels. We set $\xi_{\min} = 0.1$, $\omega_n = 3.9867$, and the restricted radius $r = 20$.

Example 4.1. For the yaw channel, combined with the fractional-order state space model (4.5), we define $x_{\psi}(t) = [x_{21}, x_{22}, x_{23}, x_{24}]^T$, then the system matrix and control matrix are

$$A_{\psi} = \begin{bmatrix} 0 & 1 & 0 & 0 \\ 0 & 0 & 1 & 0 \\ 0 & 0 & 0 & 1 \\ 0 & 0 & 0 & 0 \end{bmatrix}, B_{\psi} = \begin{bmatrix} 0 \\ 0 \\ 0 \\ 1/I_z \end{bmatrix},$$

where $I_z = 3.9062$. The MGLMI regions are given as follows:

$$\mathscr{D}_U = \mathscr{D}_{R_{1,2}}(-0.5 \pm 5.8i, 0.5) \cup \mathscr{D}_{R_3}(-6, 1) \cup \mathscr{D}_{R_4}(-19, 1).$$

From Definition 2.2, we can obtain

$$\begin{aligned} &H_{11} = 33.64, H_{12} = 0.5 + 5.8i, H_{13} = 1, H_{21} = 33.64, H_{22} = 0.5 - 5.8i, H_{23} = 1, \\ &H_{31} = 35, H_{32} = 6, H_{33} = 1, H_{41} = 360, H_{42} = 19, H_{43} = 1. \end{aligned}$$

According to Algorithm 1, the feedback control matrix F is

$$F = 10^4 \times \begin{bmatrix} -1.3524 & -0.3207 & -0.0546 & 0.0097 \end{bmatrix}$$

and it can be confirmed that $\sigma(A + BF) = \{-0.0328 \pm 5.7351, -5.4546, -19.2968\}$.

In Figure 5, we can observe that all the closed-loop eigenvalues are reassigned into the given regions. Figure 6 demonstrates the time response curve for the closed-loop fractional-order system. We can see that the feedback control matrix F obtained by multiple-region eigenvalue assignment can maintain the fractional-order quadrotor UAV system in a stable flight condition.

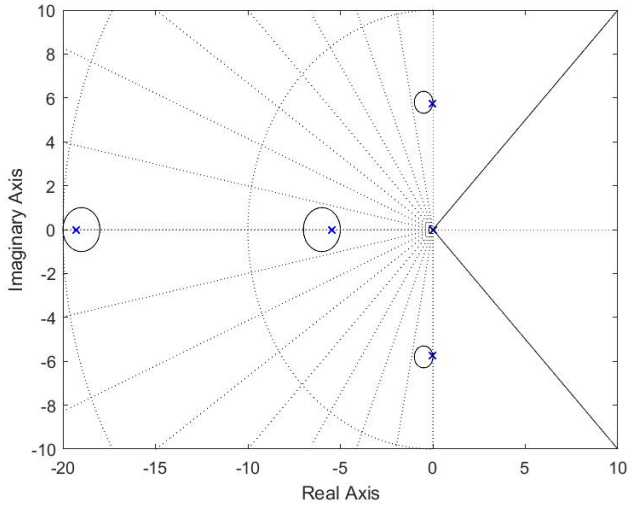

Figure 5. The closed-loop eigenvalue map of Example 4.1.

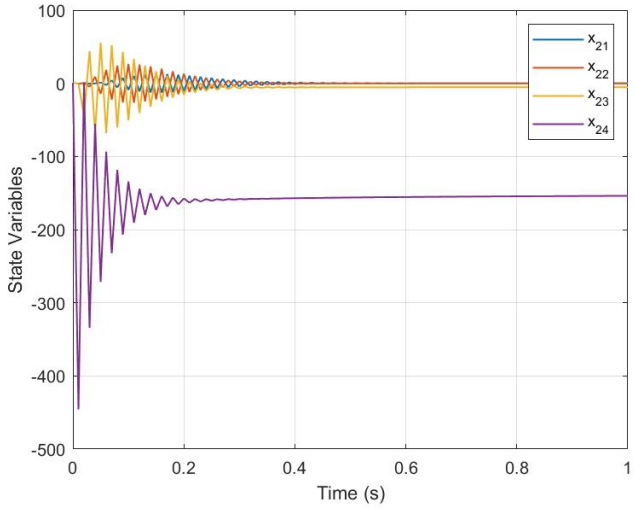

Figure 6. The closed-loop system states of Example 4.1.

Note: The system state response is $x(t) = E_{\alpha,1}(At^{\alpha})x(0) + \int_0^t (t-\tau)^{\alpha-1} E_{\alpha,\alpha}(A(t-\tau)^{\alpha})Bu(\tau)d\tau$, where $x(0)$ is the initial state, and $E_{m,n}(z) = \sum_{k=0}^{\infty} \frac{z^k}{\Gamma(mk+n)}$ is the two-parameter Mittag-Leffler function. In numerical experiments, we adopt the Grünwald-Letnikov method to compute it [41].

Example 4.2. For x-axis channels, combined with the dynamic model of the quadrotor UAV, we know that the fractional-order state space model (4.5) may be conjointly developed for roll and x-axis channels of the quadrotor UAV. Based on the earlier analysis, we can denote

$x_x(t) = [x_1, x_2, x_3, x_4, x_{17}, x_{18}, x_{19}, x_{20}]^T$, then we can obtain

$$A_x = \begin{bmatrix} 0 & 1 & 0 & 0 & 0 & 0 & 0 & 0 \\ 0 & 0 & 1 & 0 & 0 & 0 & 0 & 0 \\ 0 & 0 & 0 & 1 & 0 & 0 & 0 & 0 \\ 0 & 0 & 0 & 0 & g & 0 & 0 & 0 \\ 0 & 0 & 0 & 0 & 0 & 1 & 0 & 0 \\ 0 & 0 & 0 & 0 & 0 & 0 & 1 & 0 \\ 0 & 0 & 0 & 0 & 0 & 0 & 0 & 1 \\ 0 & 0 & 0 & 0 & 0 & 0 & 0 & 0 \end{bmatrix}, B_x = \begin{bmatrix} 0 \\ 0 \\ 0 \\ 0 \\ 0 \\ 0 \\ 0 \\ 1/I_y \end{bmatrix},$$

where $g = 9.807$ and $I_y = 4.4843$. The MGLMI regions are given as follows:

$$\mathscr{D}_U = \mathscr{D}_{R_{1,2}}(\pm 2.2i, 0.8) \cup \mathscr{D}_{R_{3,4}}(7.3 \pm 7.6i, 1.1) \cup \mathscr{D}_{R_{5,6}}(-7.3 \pm 7.6i, 1.1) \cup \mathscr{D}_{R_7}(-3.6, 1.1) \cup \mathscr{D}_{R_8}(-16, 1.1).$$

From Definition 2.2, we can obtain

$$\begin{aligned} &H_{11} = 4.2, H_{12} = +2.2i, H_{13} = 1, \\ &H_{21} = 4.2, H_{22} = -2.2i, H_{23} = 1, \\ &H_{31} = 109.84, H_{32} = -7.3 + 7.6i, H_{33} = 1, \\ &H_{41} = 109.84, H_{42} = -7.3 - 7.6i, H_{43} = 1, \\ &H_{51} = 109.84, H_{52} = 7.3 + 7.6i, H_{53} = 1, \\ &H_{61} = 109.84, H_{62} = 7.3 - 7.6i, H_{63} = 1, \\ &H_{71} = 11.75, H_{71} = 3.6, H_{72} = 1, \\ &H_{81} = 254.79, H_{82} = 16, H_{83} = 1. \end{aligned}$$

According to Algorithm 1, the feedback control matrix F is

$$F = 10^6 \times \begin{bmatrix} 2.7293 & 0.1569 & 0.3988 & 0.1387 & -0.0768 & -0.0007 & -0.0002 & -0.0001 \end{bmatrix}$$

and we can verify that

$$\sigma(A + BF) = \{-15.7757, 7.9742 \pm 8.0051i, 8.0650 \pm 7.8567i, -0.0190 \pm 2.8749i, -2.8282\}.$$

We show Figure 7 to illustrate that all the closed-loop eigenvalues are reassigned into the given regions in the fractional-order system stability region. The time response curve in Figure 8 represents the fractional-order quadrotor UAV system maintaining a stable flight performance under the proposed multiple-region eigenvalue assignment method.

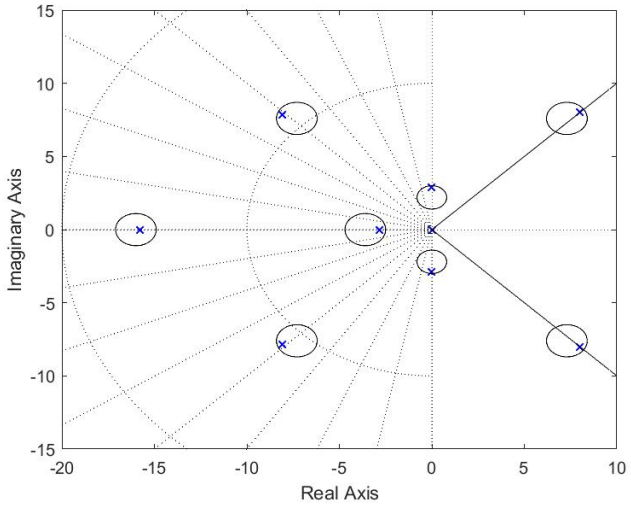

Figure 7. The closed-loop eigenvalue map of Example 4.2.

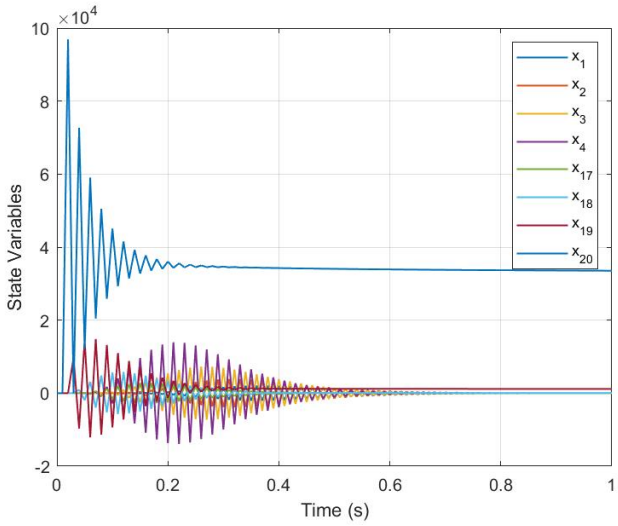

Figure 8. The closed-loop system states of Example 4.2.

4.2. Fractional-order electrical circuit systems

In the field of electrical engineering, the capacitor is regarded as an ideal component with absolutely no current flowing between the plates, based on the conventional integer-order circuit theory, since its internal resistance is considered to be infinite [42]. However, a practical capacitor has resistive losses and its resistance is finite [43]. This means that the ideal integer-order capacitor does not exist in the real world, and the actual capacitors and inductors have fractional-order properties. Fractional-order electrical circuit systems are usually a type of circuit that contains fractional-order components, such as the fractional-order capacitor and the fractional-order inductor shown in Figure 9.

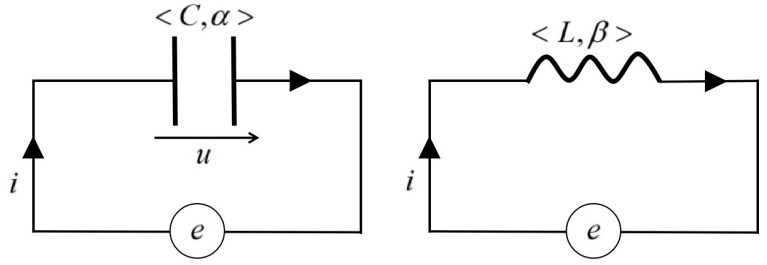

(a) Fractional order capacitor symbol (b) Fractional order inductor symbol

Figure 9. Fractional-order circuit components.

Let the current $i_C(t)$ in a fractional-order capacitor be

$$i_C(t) = D^{\alpha} q(t), 0 < \alpha < 1, \tag{4.6}$$

where C is the capacity of the capacitor and $q(t)$ is the charge. From $q(t) = Cu_C(t)$, it has

$$i_C(t) = CD^{\alpha} u_C(t), \tag{4.7}$$

where $u_C(t)$ is the voltage on the capacitor. Similarly, let the voltage $u_L(t)$ on the fractional-order inductor be

$$u_L(t) = D^{\beta} \Psi(t), 0 < \beta < 1, \tag{4.8}$$

where L is the inductance and $\Psi(t)$ is the magnetic flux of the capacitor. According to $\Psi(t) = Li_L(t)$, then

$$u_L(t) = LD^{\beta} i_L(t), \tag{4.9}$$

where $i_L(t)$ is the current in the inductor. Therefore, for a fractional-order electrical circuit composed of resistances, inductances, capacitances, and source voltages, it can be expressed as a fractional-order system by selecting appropriate voltages on the capacitors and the currents in the inductor as state variables. We will give the fractional-order electrical circuit system combined with specific electrical circuit examples [44] and explore numerical results under the proposed multiple-region eigenvalue assignment method for the fractional-order electrical circuit systems. In the following experiments, we set $\xi_{\min} = 0.1, \omega_n = 0.9980$, and the restricted radius $r = 10$.

Example 4.3. The fractional-order electrical circuit system composed of resistances R_1, R_2, R_3, R_4, inductances L_1, L_2, L_3, L_4, and source voltages e_1, e_2, e_3 is shown in Figure 10.

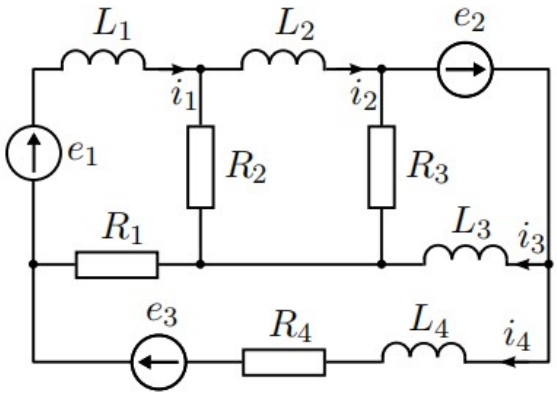

Figure 10. Fractional-order electrical circuit system.

Taking into account (4.7), (4.9), and Kirchhoff's laws, we have

$$\begin{aligned} e_1 &= (R_1 + R_2)\, i_1 - R_2 i_2 - R_1 i_4 + L_1 D^\beta i_1, \\ 0 &= -R_2 i_1 + (R_1 + R_2)\, i_2 - R_3 i_3 + L_2 D^\beta i_2, \\ e_2 &= -R_3 i_2 + R_3 i_3 + L_3 D^\beta i_3, \\ e_2 + e_3 &= -R_1 i_1 - R_3 i_2 + (R_1 + R_3 + R_4)\, i_4 + L_4 D^\beta i_4. \end{aligned} \tag{4.10}$$

Choosing the state variable to be $x(t) = \begin{bmatrix} i_1 & i_2 & i_3 & i_4 \end{bmatrix}^T$, then we can rewrite (4.10) as

$$D^\beta x(t) = Ax(t) + Bu(t),$$

where

$$A = \begin{bmatrix} -(R_1 + R_2)/L_1 & R_2/L_1 & 0 & R_1/L_1 \\ R_2/L_2 & -(R_2 + R_3)/L_2 & R_3/L_2 & 0 \\ 0 & R_3/L_3 & -R_3/L_3 & 0 \\ R_1/L_4 & R_3/L_4 & 0 & -(R_1 + R_3 + R_4)/L_4 \end{bmatrix},$$

$$B = \begin{bmatrix} 1/L_1 & 0 & 0 \\ 0 & 0 & 0 \\ 0 & 1/L_3 & 0 \\ 0 & 1/L_4 & 1/L_4 \end{bmatrix}.$$

Set $\beta = 0.85$, $L_1 = 1, L_2 = 1, L_3 = 1/3, L_4 = 1/5, R_1 = 13/10, R_2 = -1, R_3 = 13/10, R_4 = -131/10$, and the MGLMI regions

$$\mathscr{D}_U = \mathscr{D}_{R_{1,2}}(-6.7 \pm 0.1i, 0.8) \cup \mathscr{D}_{R_3}(-6.1, 0.7) \cup \mathscr{D}_{R_4}(-7.4, 0.7).$$

Then we have

$$\begin{aligned} &H_{11} = 44.74, H_{12} = 6.7 + 0.7i, H_{13} = 1, H_{21} = 44.74, H_{22} = 6.7 - 0.7i, H_{23} = 1, \\ &H_{31} = 36.72, H_{32} = 6.1, H_{33} = 1, H_{41} = 54.27, H_{42} = 7.4, H_{43} = 1. \end{aligned}$$

According to Algorithm 1, the feedback control matrix F is

$$F = \begin{bmatrix} -8.8427 & 16.4482 & 3.1147 & -1.3 \\ 9.3439 & -61.5463 & -31.0872 & 0 \\ -10.6439 & 60.2464 & 31.0872 & -44.2336 \end{bmatrix}.$$

For confirmation, we compute that $\sigma(A + BF) = \{-6.7458 \pm 0.0778i, -6.7467, -6.7467\}$. Figure 11 shows that the closed-loop eigenvalues are reassigned into the given regions $\mathscr{D}_U$. We find that the closed-loop fractional-order electrical circuit system preserves stable status under the multiple-region eigenvalue assignment method from Figure 12.

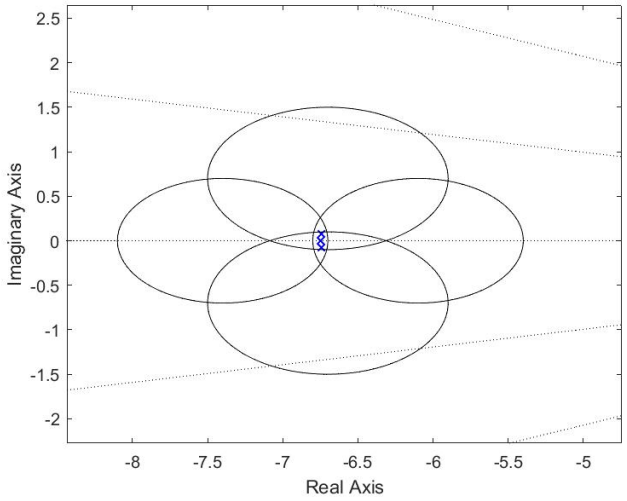

Figure 11. The closed-loop eigenvalue map of Example 4.3.

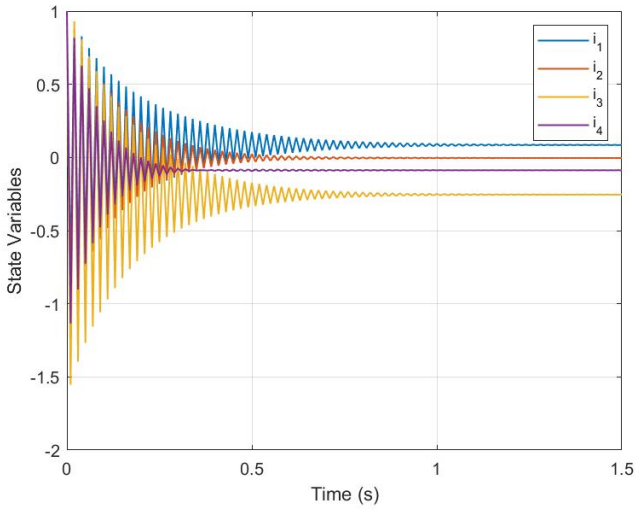

Figure 12. The closed-loop system states of Example 4.3.

Example 4.4. The fractional-order electrical circuit system composed of resistances $R_k, k = 1, \ldots, n$, capacitances $C_1, C_3, \ldots, C_{n_1}$, inductances $L_2, L_4, \ldots, L_{n_2}$, and source voltages $e_1, e_2, e_4, \ldots, e_{n_2}$ $(n = n_1 + n_2)$ is shown in Figure 13.

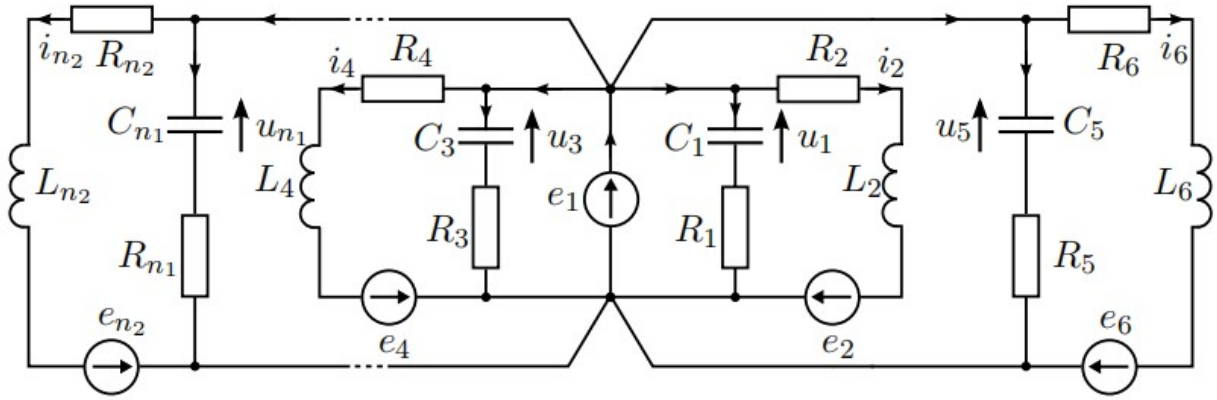

Figure 13. Fractional-order electrical circuit system.

Using Kirchhoff's laws, we can write

$$\begin{aligned} &e_1 = R_k C_k D^{\alpha} u_k + u_k, k = 1, 3, \ldots, n_1, \\ &e_1 + e_j = L_j D^{\beta} i_j + R_j i_j, j = 2, 4, \ldots, n_2. \end{aligned} \tag{4.11}$$

Assuming that $\alpha = \beta = 0.85$, we choose $x(t) = \begin{bmatrix} u_1 & u_3 & \ldots & u_{n_1} & i_2 & i_4 & \ldots & i_{n_2} \end{bmatrix}^T$ and reformulate (4.11) as

$$D^{0.85} \begin{pmatrix} u_1 \\ u_3 \\ \vdots \\ u_{n_1} \\ i_2 \\ i_4 \\ \vdots \\ i_{n_2} \end{pmatrix} = A \begin{pmatrix} u_1 \\ u_3 \\ \vdots \\ u_{n_1} \\ i_2 \\ i_4 \\ \vdots \\ i_{n_2} \end{pmatrix} + B \begin{pmatrix} e_1 \\ e_2 \\ e_4 \\ \vdots \\ e_n \end{pmatrix}, \tag{4.12}$$

where

$$A = diag \begin{pmatrix} -1/R_1C_1 & -1/R_3C_3 & \ldots & -1/R_{n_1}C_{n_1} & -R_2/L_2 & -R_4/L_4 & \ldots & -R_{n_2}/L_{n_2} \end{pmatrix} \in \mathbb{R}^{n \times n},$$

$$B = \begin{bmatrix} B_1 \\ B_2 \end{bmatrix} \in R^{n \times \left(\frac{n_2}{2}+1\right)},$$

$$B_1 = \begin{bmatrix} 1/R_1C_1 & 0 & 0 & \dots & 0 \\ 1/R_3C_3 & 0 & 0 & \dots & 0 \\ \vdots & \vdots & \vdots & \ddots & \vdots \\ -1/R_{n_1}C_{n_1} & 0 & 0 & \dots & 0 \end{bmatrix}, B_2 = \begin{bmatrix} 1/L_2 & 1/L_2 & 0 & \dots & 0 \\ 1/L_4 & 0 & 1/L_4 & \dots & 0 \\ \vdots & \vdots & \vdots & \ddots & \vdots \\ 1/L_{n_2} & 0 & 0 & \dots & 1/L_{n_2} \end{bmatrix}.$$

Set $n_1 = 9, n_2 = 2, R_1 = 1, R_3 = 1/7, R_5 = 1/2, R_7 = 5/2, R_9 = 1/3, C_1 = 1/2, C_3 = 5, C_5 = 4, C_7 = 2, R_9 = 10, R_2 = 5, L_2 = -5/2$, and the MGLMI regions

$$\mathscr{D}_U = \mathscr{D}_{R_{1,2}}(-0.55 \pm 0.05i, 0.2) \cup \mathscr{D}_{R_3}(-1.6, 0.2) \cup \mathscr{D}_{R_4}(-0.4, 0.1) \cup \mathscr{D}_{R_5}(-1, 0.2) \cup \mathscr{D}_{R_6}(-0.3, 0.1).$$

From Definition 2.2, we can get

$$\begin{aligned} &H_{11} = 0.265, H_{12} = 0.55 - 0.05i, H_{13} = 1, H_{21} = 0.265, H_{22} = 0.55 + 0.05i, H_{23} = 1, \\ &H_{31} = 2.52, H_{32} = 1.6, H_{33} = 1, H_{41} = 0.15, H_{42} = 0.4, H_{43} = 1, \\ &H_{51} = 0.96, H_{52} = 1, H_{53} = 1, H_{61} = 0.08, H_{62} = 0.3, H_{63} = 1. \end{aligned}$$

According to Algorithm 1, the feedback control matrix F is

$$F = \begin{bmatrix} 0.3385 & 0.1607 & -0.0531 & -0.0179 & -0.0278 & 0 \\ -0.3385 & -0.1607 & 0.0531 & 0.0179 & 0.0278 & 7.1055 \end{bmatrix}$$

and $\sigma(A + BF) = \{-1.6527, -0.2059, -0.3165, -0.6857 \pm 0.0193i, -0.8422\}$. Numerical results are shown in Figures 14 and 15, where we can see that the stability and region constraint requirements are achieved.

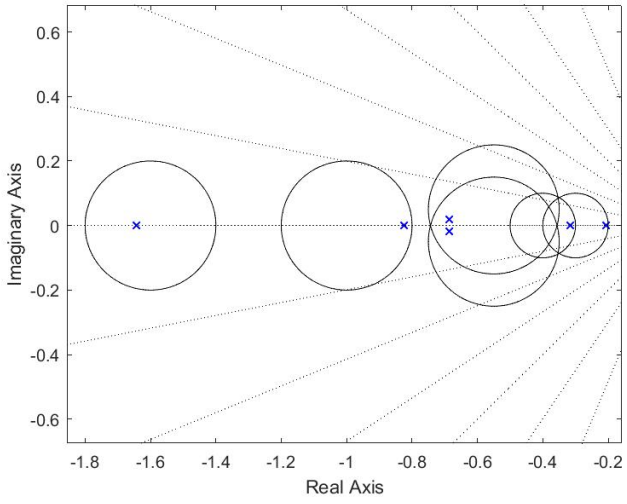

Figure 14. The closed-loop eigenvalue map of Example 4.4.

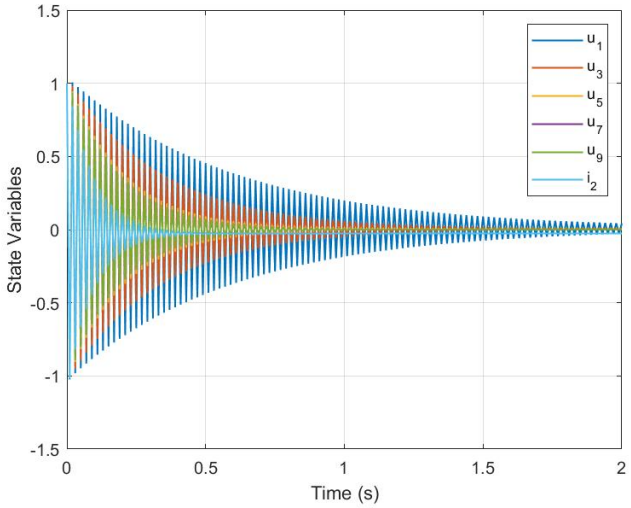

Figure 15. The closed-loop system states of Example 4.4.

4.3. Fractional-order rotary inverted pendulum system

By utilizing the inverted pendulum model, we illustrate the functionality and applicability of the proposed method. The transfer function of the fractional-order rotary inverted pendulum system is

$$G(s) = \left(b_0 + b_1 s^{\alpha} + b_2 s^{2\alpha}\right) \Big/ \left(1 + a_1 s^{\alpha} + a_2 s^{2\alpha} + a_3 s^{3\alpha} + a_4 s^{4\alpha}\right). \tag{4.13}$$

According to the system identification method and results of [45], we know that the fractional-order model is closer to the actual model when the fractional order is α= 0.7 with $a_1 = 0.0107, a_2 = -0.0227$, $a_3 = -0.0179, a_4 = 0, b_1 = -0.226, b_2 = b_3 = 0$. Therefore, the fractional-order state space model of the circular inverted pendulum is given as follows:

$$D^{0.7} x(t) = Ax(t) + Bu(t), \tag{4.14}$$

where

$$A = \begin{bmatrix} 0 & 1 & 0 \\ 0 & 0 & 1 \\ 55.8569 & 0.5978 & -1.2682 \end{bmatrix}, B = \begin{bmatrix} 0 \\ 0 \\ 1 \end{bmatrix}.$$

We set $\xi_{\min} = 0.1, \omega_n = 1.7804$, and the restricted radius $r = 15$.

Example 4.5. [45] Giving the fractional-order system (4.14) and the following MGLMI regions

$$\mathscr{D}_U = \mathscr{D}_{R_{1,2}}(-1 \pm 2i, 0.5) \cup \mathscr{D}_{R_3}(-4, 1).$$

From Definition 2.2, it yields that

$$\begin{aligned} &H_{11} = 4.75, H_{12} = 1 + 2i, H_{13} = 1, \\ &H_{21} = 4.75, H_{22} = 1 - 2i, H_{23} = 1, \\ &H_{31} = 15, H_{32} = 4, H_{33} = 1. \end{aligned}$$

According to Algorithm 1, the feedback control matrix F is

$$F = \begin{bmatrix} -71.6948 & -11.9251 & -4.2498 \end{bmatrix},$$

and $\sigma(A + BF) = \{-0.9630 \pm 1.8660i, -3.5920\}$. Figure 16 implies that the closed-loop eigenvalues are assigned into the specified regions. The validity of the proposed method is assessed by a comparison experiment between the multiple-region eigenvalue assignment method and the single-region method, as shown in Figures 17 to 19. The closed-loop system states of these two methods are shown in Figures 17 to 19. The fluctuations of the system states using the multiple-region eigenvalue assignment method are small, and the method has desired stability, showing that this method has better effectiveness.

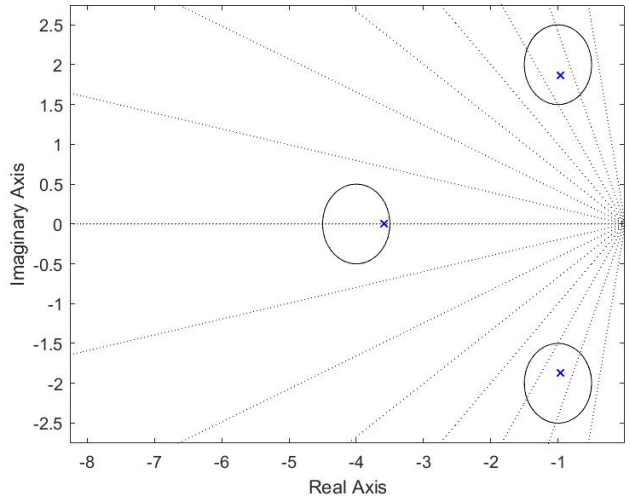

Figure 16. The closed-loop eigenvalue map of Example 4.5.

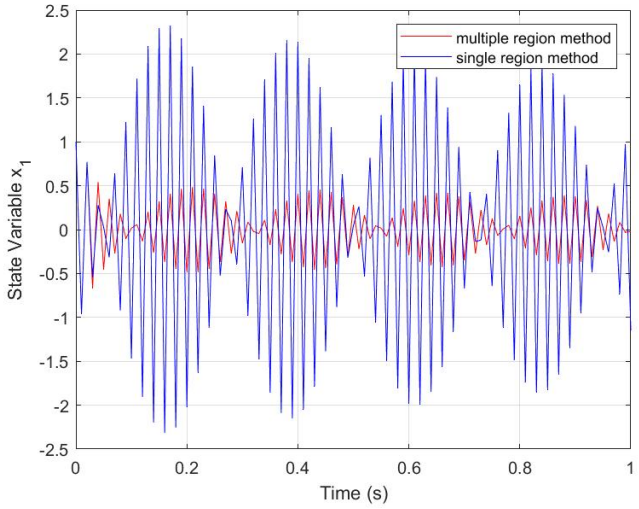

Figure 17. The closed-loop system state of x_1.

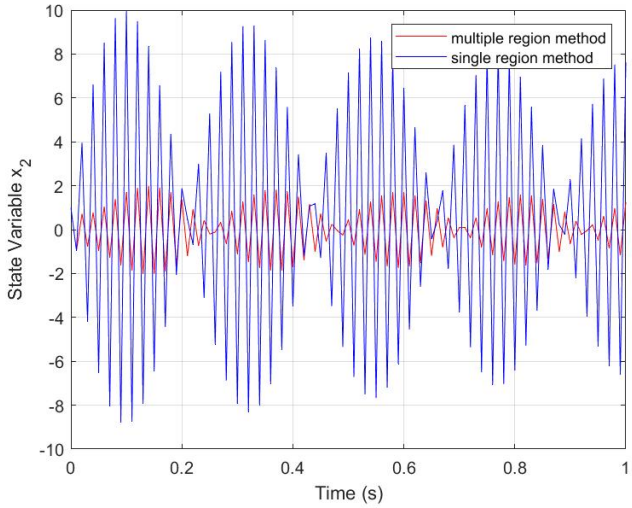

Figure 18. The closed-loop system state of x_2.

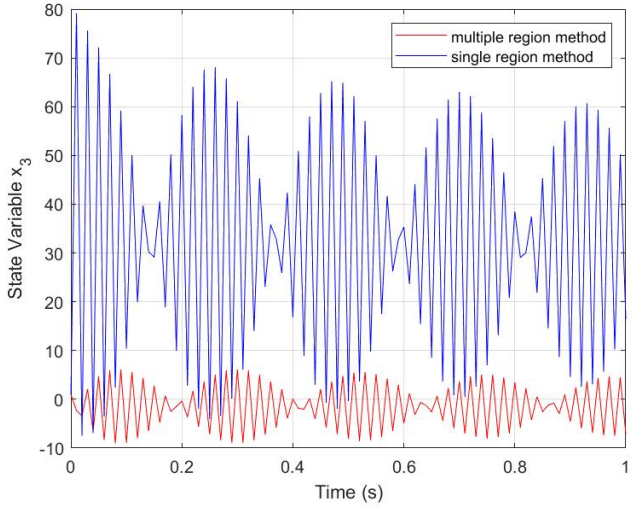

Figure 19. The closed-loop system state of x_3.

5. Conclusions

In this work, active vibration control for fractional-order systems based on multiple-region eigenvalue assignment is considered. We first propose the selection criteria of fractional-order multiple stability regions and give the definition of multiple regions according to linear matrix inequality theory. Based on the inverse eigenvalue problem theory, the sufficient condition for solving the feedback control matrix under the multiple-region eigenvalue assignment is provided, and the expression of the solution is given. Then, we present a numerical algorithm for solving this problem, which improves control performance. Numerical experiments of fractional-order quadrotor UAV

systems, fractional-order electrical circuit systems, and fractional-order rotary inverted pendulum systems show the feasibility of our algorithm. However, the method is only applicable for fractional-order systems without uncertain disturbances. In future work, other vibration control methods like PID control, may be considered.

Use of AI tools declaration

The authors declare they have not used Artificial Intelligence (AI) tools in the creation of this article.

Acknowledgments

This research was supported in part by National Natural Science Foundation of China (Nos. 11401305 and 11571171) and Shenzhen Science and Technology Program (No. JCYJ20230807142002006).

Conflict of interest

The authors declare there is no conflict of interest.

References

1. R. F. Meng, D. S. Yin, C. S. Drapaca, A variable order fractional constitutive model of the viscoelastic behavior of polymers, *Int. J. Non-Linear Mech.*, **113** (2019), 171–177. https://doi.org/10.1016/j.ijnonlinmec.2019.04.002
2. I. E. Saçu, A practical synthesis and analysis of the fractional-order FitzHugh-Nagumo neuronal model, *J. Comput. Electron.*, **23** (2024), 188–207. https://doi.org/10.1007/s10825-023-02120-x
3. Q. Zhang, K. Z. Wei, A comparative study of fractional-order models for supercapacitors in electric vehicles, *Int. J. Electrochem. Sci.*, **19** (2024), 100441. https://doi.org/10.1016/j.ijoes.2023.100441
4. J. Espinoza, N. Hakim, D. Tan, T. Wilson, K. Bingi, E. Khan, et al., Fractional-order PID control of quadrotor drone, in *2023 Innovations in Power and Advanced Computing Technologies(i-PACT)*, IEEE, (2023), 1–6. https://doi.org/10.1109/i-PACT58649.2023.10434503
5. Z. Li, Optical solutions of the nonlinear Kodama equation with the M-truncated derivative via the extended (G'/G)-expansion method, *Fractal Fract.*, **9** (2025), 300. https://doi.org/10.3390/fractalfract9050300
6. Z. Li, Y. Y. Jiang, Bifurcation, chaotic behavior, and traveling wave solutions for the fractional (4+1)-dimensional Davey–Stewartson–Kadomtsev–Petviashvili model, *Open Phys.*, **23** (2025), 20250157. https://doi.org/10.1515/phys-2025-0157
7. K. Farooq, A. H. Tedjani, Z. Li, E. Hussain, Soliton dynamics of the nonlinear Kodama equation with M-truncated derivative via two innovative schemes: The generalized Arnous method and the Kudryashov method, *Fractal Fract.*, **9** (2025), 436. https://doi.org/10.3390/fractalfract9070436

8. H. S. Li, Y. Luo, Y. Q. Chen, A fractional-order proportional and derivative (FOPD) motion controller: Tuning rule and experiments, *IEEE Trans. Control Syst. Technol.*, **18** (2010), 516–520. https://doi.org/10.1109/TCST.2009.2019120

9. R. L. Magin, Fractional calculus in bioengineering, part 1, *Crit. Rev. Biomed. Eng.*, **32** (2004), 1–104. https://doi.org/10.1615/critrevbiomedeng.v32.i1.10

10. X. F. Zhang, C. Lin, Y. Q. Chen, D. Boutat, A unified framework of stability theorems for LTI fractional order systems with $0 < \alpha < 2$, *IEEE Trans. Circuits Syst. II Express Briefs*, **67** (2020), 3237–3241. https://doi.org/10.1109/TCSII.2020.2978869

11. A. Kyprianou, J. E. Mottershead, H. J. Ouyang, Assignment of natural frequencies by an added mass and one or more springs, *Mech. Syst. Signal Process.*, **18** (2004), 263–289. https://doi.org/10.1016/S0888-3270(02)00220-0

12. K. Farahani, H. Bahai, An inverse strategy for relocation of eigenfrequencies in structural design Part I: First order approximate solutions, *J. Sound Vib.*, **274** (2004), 481–505. https://doi.org/10.1016/j.jsv.2003.11.009

13. Y. M. Ram, J. E. Mottershead, Receptance method in active vibration control, *AIAA J.*, **45** (2007), 562–567. https://doi.org/10.2514/1.24349

14. Y. Yuan, Y. Lu, X. J. Ma, J. L. Li, H. Y. Yue, Distributed active vibration control for helicopter based on diffusion collaboration, *Chin. J. Aeronaut.*, **37** (2024), 208–232. https://doi.org/10.1016/j.cja.2024.04.006

15. Q. Zhang, S. Y. Han, M. A. El-Meligy, M. Tlija, Active control vibrations of aircraft wings under dynamic loading: Introducing PSO-GWO algorithm to predict dynamical information, *Aerosp. Sci. Technol.*, **153** (2024), 109430. https://doi.org/10.1016/j.ast.2024.109430

16. S. Zhang, L. Liu, X. M. Zhang, Y. K. Zhou, Q. Yang, Active vibration control for ship pipeline system based on PI-LQR state feedback, *Ocean Eng.*, **310** (2024), 118559. https://doi.org/10.1016/j.oceaneng.2024.118559

17. P. L. Xu, X. Lan, C. J. Zeng, J. S. Leng, Y. J. Liu, Active vibration control effect of 3D printed cruciform honeycomb laminates based on fiber-reinforced shape memory polymer, *Compos. Struct.*, **346** (2024), 118415. https://doi.org/10.1016/j.compstruct.2024.118415

18. Y. Q. Tian, C. Zhang, L. Yang, Active control of vibration and radiated noise in the shaft-shell coupled system of an underwater vehicle, *Appl. Ocean Res.*, **154** (2025), 104324. https://doi.org/10.1016/j.apor.2024.104324

19. A. O. Adelakun, S. T. Ogunjo, Active control and electronic simulation of a novel fractional order chaotic jerk system, *Commun. Nonlinear Sci.*, **130** (2024), 107734. https://doi.org/10.1016/j.cnsns.2023.107734

20. M. H. Kazemi, R. Tarighi, PID-based attitude control of quadrotor using robust pole assignment and LPV modeling, *Int. J. Dynam. Control*, **12** (2024), 2385–2397. https://doi.org/10.1007/s40435-023-01372-6

21. C. C. Ku, W. J. Chang, C. Y. Yen, G. W. Chen, Gain-scheduled controller design for linear parameter varying systems subject to pole assignment, *Optim. Control Appl. Methods*, **41** (2020), 1439–1450. https://doi.org/10.1002/oca.2606

22. S. J. Zhang, Z. D. Wang, D. R. Ding, H. S. Shu, T. Hayat, A. M. Dobaie, On design of robust fault detection filter in finite-frequency domain with regional pole assignment, *IEEE Trans. Circuits Syst. II Express Briefs*, **62** (2015), 382–386. https://doi.org/10.1109/TCSII.2014.2387684

23. D. Richiedei, I. Tamellin, Active control of linear vibrating systems for antiresonance assignment with regional pole placement, *J. Sound Vib.*, **494** (2020), 115858. https://doi.org/10.1016/j.jsv.2020.115858

24. P. Schaub, P. Vogt, U. Konigorski, Robust coupling control using pole region assignment, *Syst. Control Lett.*, **158** (2021), 105067. https://doi.org/10.1016/j.sysconle.2021.105067

25. A. Ç. Arıcan, E. H. Çopur, G. Inalhan, M. U. Salamci, State dependent regional pole assignment controller design for a 3-DOF helicopter model, in *2023 International Conference on Unmanned Aircraft Systems(ICUAS)*, IEEE, (2023), 1067–1072. https://doi.org/10.1109/ICUAS57906.2023.10155816

26. A. C. Arıcan, E. H. Copur, G. Inalhan, M. U. Salamci, An extension algorithm of regional eigenvalue assignment controller design for nonlinear systems, *Aerospace*, **10** (2023), 893. https://doi.org/10.3390/aerospace10100893

27. T. T. Zhang, H. S. Zhang, X. P. Xie, Region stability/stabilization and H_∞ control for discrete-time impulsive Takagi–Sugeno fuzzy systems, *IEEE Trans. Fuzzy Syst.*, **32** (2024), 3410–3419. https://doi.org/10.1109/TFUZZ.2024.3372936

28. H. S. Zhang, Y. E. Li, X. P. Xie, J. W. Xia, A novel stability criterion and precise control for linear time delay systems based on regional configuration of the poles, *ISA Trans.*, **148** (2024), 349–357. https://doi.org/10.1016/j.isatra.2024.03.008

29. P. H. He, H. S. Zhang, S. F. Su, A sliding mode control method with variable convergence rate for nonlinear impulsive stochastic systems, *IEEE Trans. Cybern.*, **55** (2025), 2213–2222. 10.1109/TCYB.2025.3551668

30. S. X. Xiong, M. T. Chen, Z. Q. Wei, Tracking flight control of UAV based on multiple regions pole assignment method, *Aerosp. Sci. Technol.*, **129** (2022), 107848. https://doi.org/10.1016/j.ast.2022.107848

31. D. Peaucelle, D. Arzelier, O. Bachelier, J. Bernussou, A new robust D-stability condition for real convex polytopic uncertainty, *Syst. Control Lett.*, **40** (2000), 21–30. https://doi.org/10.1016/S0167-6911(99)00119-X

32. D. Matignon, Stability results for fractional differential equations with applications to control processing, *Comput. Eng. Syst. Appl.*, **2** (1996), 963–968.

33. O. Zarrag, I. Sarría, J. García-Barruetabeña, F. Cortés, An analysis of the dynamical behaviour of systems with fractional damping for mechanical engineering applications, *Symmetry*, **11** (2019), 1499. https://doi.org/10.3390/sym11121499

34. L. Yu, *Robust Control: Linear Matrix Lnequality Approach*, Tsinghua University Press, Beijing, China, 2002.

35. B. W. Xu, R. Blok, P. Teuffel, An investigation of the effect of relative humidity on viscoelastic properties of flax fiber reinforced polymer by fractional-order viscoelastic model, *Compos. Commun.*, **37** (2023), 101406. https://doi.org/10.1016/j.coco.2022.101406

36. Y. J. Wang, G. H. Zhao, A comparative study of fractional-order models for lithium-ion batteries using Runge Kutta optimizer and electrochemical impedance spectroscopy, *Control Eng. Pract.*, **133** (2023), 105451. https://doi.org/10.1016/j.conengprac.2023.105451
37. P. Anbalagan, Y. H. Joo, Stabilization analysis of fractional-order nonlinear permanent magnet synchronous motor model via interval type-2 fuzzy memory-based fault-tolerant control scheme, *ISA Trans.*, **142** (2023), 310–324. https://doi.org/10.1016/j.isatra.2023.08.021
38. A. W. A. Saif, K. B. Gaufan, S. El-ferik, M. Al-dhaifallah, Fractional order sliding mode control of quadrotor based on fractional order model, *IEEE Access*, **11** (2023), 79823–79837. https://doi.org/10.1109/ACCESS.2023.3296644
39. S. Y. Xi, Z. H. Chen, Z. H. Chen, Y. Chen, Trajectory tracking of fractional order quadrotor UAV based on adaptive fuzzy fractional order PID controller, in *2024 14th Asian Control Conference (ASCC)*, IEEE, (2024), 2054–2059.
40. R. Austin, *Unmanned Aircraft Systems: UAVs Design, Development and Deployment*, Wiley, 2010. https://doi.org/10.1002/9780470664797
41. D. Y. Xue, *Fractional Calculus: Nemerical Algorithms and Implimentations*, Tsinghua University Press, Beijing, China, 2023.
42. B. Zhang, X. J. Shu, *Fractional-Order Electrical Circuit Theory*, Springer, 2022. https://doi.org/10.1007/978-981-16-2822-1
43. H. Matsumori, K. Urata, T. Shimizu, K. Takano, H. Ishii, Capacitor loss analysis method for power electronics converters, *Microelectron. Reliab.*, **88–90** (2018), 443–446. https://doi.org/10.1016/j.microrel.2018.07.049
44. T. Kaczorek, K. Rogowski, *Fractional Linear Systems and Electrical Circuits*, Springer, 2015. https://doi.org/10.1007/978-3-319-11361-6
45. T. Y. Yang, *Robust Pole Assignment for Fractional-Order Control Systems via Neurodynamic Optimization (in Chinese)*, Master Thesis, Dalian University of Technology, 2018.

Appendix

A1. Construction of the matrix T_k in (3.9)

A sequence of invertible matrices T_k is defined as

$$T_k = \begin{bmatrix} T_{k_1} & & & \\ & \ddots & & \\ & & T_{k_{s-1}} & \\ & & & T_{k_s} \end{bmatrix},$$

where T_{k_r} $(r = 1, \ldots, s)$ is the diagonal block invertible matrix, and

$$T_{k_r} = \begin{bmatrix} k^{n_r-1} & & & \\ & \ddots & & \\ & & k & \\ & & & 1 \end{bmatrix} (k \neq 0).$$

Thus we have

$$T_{k_r}^{-1} = \begin{bmatrix} k^{-(n_r-1)} & & & \\ & \ddots & & \\ & & k^{-1} & \\ & & & 1 \end{bmatrix}.$$

According to (3.7) in the proof of Theorem 3.1, let $\Lambda_r = T_{k_r}^{-1} J_r T_{k_r}$, it yields that

$$\Lambda_r = \begin{bmatrix} \lambda_r & k^{-1} & & & \\ & \lambda_r & k^{-1} & & \\ & & \ddots & \ddots & \\ & & & \lambda_r & k^{-1} \\ & & & & \lambda_r \end{bmatrix}.$$

Then we can compute

$$\begin{aligned} & T_k^{-1} J T_k \\ &= \begin{bmatrix} T_{k_1} & & & \\ & \ddots & & \\ & & T_{k_{s-1}} & \\ & & & T_{k_s} \end{bmatrix}^{-1} \begin{bmatrix} J_1 & & & \\ & \ddots & & \\ & & J_{s-1} & \\ & & & J_s \end{bmatrix} \begin{bmatrix} T_{k_1} & & & \\ & \ddots & & \\ & & T_{k_{s-1}} & \\ & & & T_{k_s} \end{bmatrix} \\ &= \begin{bmatrix} T_{k_1}^{-1} J_1 T_{k_1} & & & \\ & \ddots & & \\ & & T_{k_{s-1}}^{-1} J_{s-1} T_{k_{s-1}} & \\ & & & T_{k_s}^{-1} J_s T_{k_s} \end{bmatrix} \\ &= \begin{bmatrix} \Lambda_1 & & & \\ & \ddots & & \\ & & \Lambda_{s-1} & \\ & & & \Lambda_s \end{bmatrix}. \end{aligned}$$

According to (3.8), it can be concluded that

$$\lim_{k\to\infty} T_k^{-1} J T_k = \lim_{k\to\infty} diag\{\Lambda_1, \ldots, \Lambda_s\} = diag\{\lambda_1 I_{n_1}, \ldots, \lambda_s I_{n_s}\} = \Lambda.$$